
Article:
Hadjisolomou, P., Shaisultanov, R., Jeong, T. M. et al. (2025) High-energy photon generation from self-organized plasma cavities in field-enhanced laser-preplasma interactions. Physical Review Research. 043275. ISSN: 2643-1564

https://doi.org/10.1103/b2p6-t548

High-energy photon generation from self-organized plasma cavities in field-enhanced laser-preplasma interactions

P. Hadjisolomou [1,*] R. Shaisultanov,[1] T. M. Jeong [1] C. P. Ridgers [2] and S. V. Bulanov [1]
[1]ELI Beamlines Facility, Extreme Light Infrastructure ERIC, Za Radnicí 835, 25241 Dolní Břežany, Czech Republic
[2]York Plasma Institute, Department of Physics, University of York, Heslington, York, North Yorkshire YO10 5DD, United Kingdom

(Received 7 August 2025; accepted 21 October 2025; published 9 December 2025)

The interaction of an ultraintense Nd:glass laser pulse with a near-critical plasma self-organizes into a highly efficient γ-ray source. Three-dimensional particle-in-cell simulations demonstrate that relativistic self-focusing, aided by a self-generated electron cavity, enhances the laser intensity by more than an order of magnitude, driving the system into the radiation-reaction-dominated regime, i.e., one where the electrons lose a substantial amount of their energy as hard radiation. Peak photon emission occurs near 0.5 times the relativistic critical density, with a γ-photon yield exceeding 20% of the laser energy. Compared to Ti:Sa lasers of the same power, the longer duration of Nd:glass laser pulses leads to an order of magnitude increase in γ-photon number in the extreme conversion efficiency regime, making them particularly well suited for photonuclear physics applications. These findings point to a robust and scalable mechanism for compact, ultrabright γ-ray generation in the multipetawatt regime.

DOI: 10.1103/b2p6-t548

I. INTRODUCTION

Ultraintense laser-plasma interactions at multipetawatt power levels are rapidly advancing [1] into regimes where radiation reaction and quantum electrodynamics (QED) effects play a central role in shaping plasma dynamics [2,3]. At intensities exceeding $10^{22}\,\mathrm{W\,cm^{-2}}$, electrons emit "high-energy" γ photons with energy $>1\,\mathrm{MeV}$ (hereafter referred to simply as "photons" for brevity) via nonlinear Compton scattering, and the related radiation losses strongly influence their dynamics [4–7]. These interactions hold promise for producing compact, ultrabright γ-ray sources [8] relevant to photonuclear physics [9–11], laboratory astrophysics [12–16], and fundamental tests of strong-field QED [2,17,18]. Here, brightness is the main constraint, and we demonstrate how it can be increased by an order of magnitude, thereby enabling these applications in the near term.

Previous studies have shown that in near-critical plasmas within the regime of relativistic transparency, a self-organized channel can be formed [19,20]. When it comes to photon generation, efficient regimes were found by employing tightly focused pulses [21,22], idealized preformed channels [23], or engineered target concepts such as reflectors and bilayer targets [24–26]. However, simplified experimental arrangements dictate the use of robust targets, typically accompanied by a preplasma profile [27–29]. The combined effects of relativistic self-focusing, cavity formation, and radiation-reaction feedback remain incompletely understood under realistic conditions involving kilojoule-class, moderately focused laser pulses of long duration, such as Nd:glass laser pulses [30,31]. This work demonstrates that high photon yield and strong laser-to-photon coupling can be achieved at intensities and configurations available with kilojoule-class systems, making experimental realization feasible without requiring tightly focused or ultrashort pulses.

As the laser pulse propagates through the near-critical plasma, it undergoes relativistic self-focusing due to intensity-dependent changes in the refractive index [32–35]. This process leads to the formation of a self-generated electron cavity: a low-density channel carved out by the ponderomotive force, the microscopic mechanism whose macroscopic manifestation is the radiation pressure that transfers momentum to the plasma. A useful physical framework for understanding this initial stage of cavity formation is provided by a "snowplow" model [36,37], wherein the intense laser field effectively sweeps up plasma electrons and compresses them into a narrow density front. This compression generates a space-charge field that pulls ions outward, setting up a comoving double layer and initiating a collective plasma motion. The snowplow model captures the quasisteady balance between the laser radiation pressure and plasma inertia, leading to a forward-moving electron-depleted channel. This process initiates cavity formation and continues to shape the plasma structure until instabilities and magnetic-field-driven plasma restructuring effects dominate.

In this article, we present three-dimensional (3D) particle-in-cell (PIC) simulations of a 10 PW Nd:glass laser pulse (of dimensionless field amplitude $a_0 = e\,E/(m_e\,c\,\omega) \approx 80$, where E is the laser electric field, e is the elementary charge, m_e is the electron mass, c is the speed of light in vacuum, and ω is the laser frequency) interacting with a (relativistically) near-critical plasma of a hyperbolic tangent density profile.

*Contact author: Prokopis.Hadjisolomou@eli-beams.eu

We show that relativistic self-focusing and cavity formation enhance the laser field by more than an order of magnitude, entering the radiation-reaction- dominated regime at approximately ten times lower laser intensity than expected [38]. Peak γ-ray emission occurs near $0.5\,n_{\rm cr}$ (the relativistic critical electron density is $n_{\rm cr} = \gamma\,\epsilon_0\,m_e\,\omega^2/e^2$, where ϵ_0 is the vacuum permittivity and $\gamma \approx \sqrt{1+a_0^2/2}$ for a linearly polarized laser), with excess of 20% of the laser energy converted into high-energy photons. These findings establish a robust and experimentally accessible mechanism for generating ultrabright γ-ray sources using multipetawatt laser systems.

II. SIMULATION SETUP

We use the 3D QED-PIC code epoch [39] to simulate the interaction of a laser of $\mathcal{E}_{\rm las} = 1500\,$J energy and 150 fs duration (at full width at half maximum—FWHM) with a near-critical plasma. A characteristic wavelength of 1.06 μm for Nd:glass systems is used. The laser is linearly polarized and focused to a 10 μm spot size (at FWHM), giving a vacuum peak intensity of $8.3\times10^{21}\,\mathrm{W\,cm^{-2}}$. The target consists of fully ionized plasma (mass to atomic number ratio of 2) with a hyperbolic tangent electron density profile of the form

$$n_e = \frac{n_{e0}}{2}\left[1+\tanh\left(\frac{x-x_0}{w_0}\right)\right], \tag{1}$$

with optimal (for photon emission) $x_0 = 98.304\,\mu$m, $w_0 = 30\,\mu$m, and $n_{e0} = 3.28\times10^{28}\,\mathrm{m^{-3}} \approx 0.56\,n_{\rm cr}$; this density corresponds to the bulk density of silica eerogel [40–42]; the hyperbolic tangent density profile models the preplasma front. Thus, the bulk aerogel medium and the preplasma gradient together represent one consistent experimental configuration. The laser focal spot coincides with the location where $n_e = 0.5\,n_{e0}$ (at $x = x_0$), with the laser pulse propagating along the x axis and its electric field oscillating along the y axis. The simulation box spans from 0 to 196.608 μm in the x direction and from −24.576 to 24.576 μm in the other two directions. The x direction is resolved with 16 nm and the others with 128 nm cells, with each cell containing two macroelectrons and two macroions. The Gaussian laser pulse is initialized such that its peak reaches the left simulation boundary after a delay of three standard deviations σ. The simulations use the QED modules of epoch [5], which include nonlinear Compton scattering with stochastic radiation reaction and photon emission, together with Breit-Wheeler pair production (though the latter is negligible under the present conditions). The Higuera-Cary particle pusher [43] was employed.

III. RESULTS AND DISCUSSION

Relativistic transparency enables partial penetration of the laser into the plasma. As the laser pulse sweeps electrons forward and expels them transversely, a strong longitudinal electrostatic field is established, enabling pre-acceleration and guiding conditions for electrons [19,44]. Relativistic self-focusing leads to the formation of a narrow, electron-depleted channel. The early stages of this channel formation are consistent with the snowplow model, where the laser front accumulates and compresses electrons into a thin shell around an ion channel, establishing strong electrostatic fields that contribute to charge separation and ion motion. Following Ref. [36], the cavity boundary is obtained within the snowplow model under the assumptions of quasistatic ion motion, transverse electron expulsion at the laser front, and cylindrical symmetry. The resulting expression reads

$$\frac{r}{\lambda^3}\sqrt{r^4+s^4} - \frac{1}{2}F\left[\mathrm{acos}\left(\frac{r^2-s^2}{r^2+s^2}\right),\frac{\sqrt{2}}{2}\right] + 3\frac{s^2\,c}{\lambda^3 v_g}(x-v_g t) = C, \tag{2}$$

where $r=\sqrt{y^2+z^2}$ is the cavity radius, v_g is the group velocity, t is the propagation time, $F(u,\kappa)$ is the elliptic integral of the first kind, $s = r_0\sqrt{p_0/(m_i\,c)}$, m_i is the ion mass, p_0 is ion momentum, r_0 is the laser waist, and C is a constant. For linear polarization, we have $s = r_0\sqrt{a_i/\sqrt{2}}$, where $a_i = a_0\,m_e/m_i$. Since at the cavity front $x = v_g t$ and $r = 0$, then $C = \frac{1}{2}\,\mathrm{F}(\pi,\frac{\sqrt{2}}{2})$.

However, self-focusing plays an important role in cavity evolution, which we acknowledge by modifying

$$s(x) = s_0\,r(x)\,f(x)^{1/4}\,a(x)^{1/2}, \tag{3}$$

where $s_0 = 3$ serves as a fitting coefficient. Initially, we assume that self-focusing produces a truncated conical cavity, of the smaller cone diameter equal to λ. Thus,

$$r(x) = r_0 - (r_0-\lambda)\frac{x}{v_g t}. \tag{4}$$

Second, by assuming the pulse is long enough and that the power flow through two planes orthogonal to the propagation direction is conserved, we add a second correction term for field intensification within the cone, as

$$a(x) = \frac{a_i}{\sqrt{2}}\frac{r_0}{r(x)}. \tag{5}$$

Third, we acknowledge reduction of the pulse energy during cavity formation, through fitting to the numerical data for energy,

$$f(x) = \mathcal{E}_{\rm min}/\mathcal{E}_{\rm las} + \frac{1-\mathcal{E}_{\rm min}/\mathcal{E}_{\rm las}}{1+\exp[(x-x_c)/d]}, \tag{6}$$

with fitting coefficients $\mathcal{E}_{\rm min}\approx 141\,$J, $x_c \approx 116\,\mu$m, and $d \approx 17.7\,\mu$m. This coherent pushing action results in the initial shaping of the cavity before transverse and longitudinal instabilities fully develop. The formation of this cavity is visible in Fig. 1, where the fitted cavity walls are represented by the red line.

The cavity confines the laser energy, as evident in Fig. 2, where the peak field intensity inside the plasma (black curve) rises to $\sim 2\times10^{23}\,\mathrm{W\,cm^{-2}}$, corresponding to $a_0 \approx 400$, compared with the initial vacuum value of $\sim 8\times10^{21}\,\mathrm{W\,cm^{-2}}$ ($a_0 \approx 80$, gray shaded band). This represents an intensity enhancement of approximately 25 times due to relativistic self-focusing and cavity confinement. However, as electrons reach ultrarelativistic energies, radiation reaction alters their trajectories, reduces dephasing length, and suppresses further energy gain [45], ultimately limiting electron maximum energy $\mathcal{E}_{\rm max}$ to a few GeV despite the extreme field strength. This interplay between snowplow-driven cavity formation and

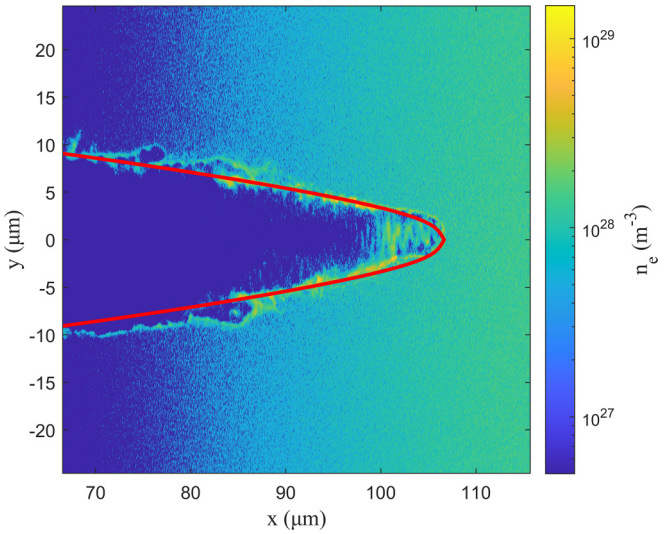

FIG. 1. Electron number density in the xy plane at 500 fs simulation time. The laser expels electrons transversely via the ponderomotive force, forming a self-organized, electron-depleted cavity that guides the laser over extended distances. The red line shows a fit to the cavity boundary using Eqs. (2)–(6), capturing the balance between laser radiation pressure and plasma response. This structure facilitates field intensification, thus enhancing photon emission.

electron acceleration under strong radiation damping governs the electron dynamics and, by extension, the photon emission spectrum. In the high-electron-energy limit of near-vacuum laser electron acceleration, the maximum electron energy gain is governed by the scaling $\mathcal{E}_{\max} \approx 31\sqrt{P\,(\mathrm{TW})}\,\mathrm{MeV}$, where P is the laser power [46]. For a laser power of $P = 10\,\mathrm{PW}$, this yields an upper-bound energy gain of approximately $\mathcal{E}_{\max} \approx 3.1\,\mathrm{GeV}$. This estimate represents the ideal scenario in which electrons are injected with sufficiently high energy to avoid

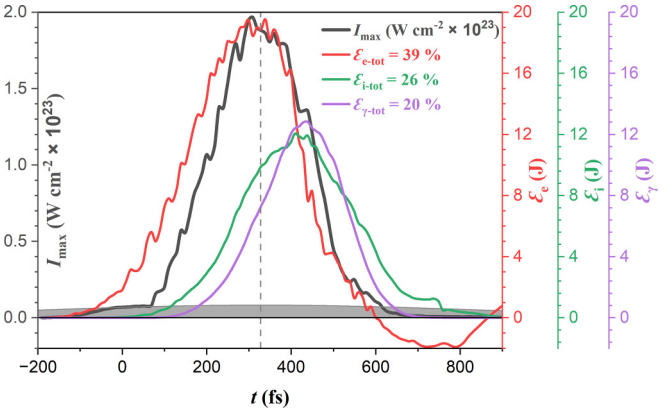

FIG. 2. Left axis: Temporal evolution (shifted by 3σ) of the peak laser intensity in plasma (black solid line) compared with the corresponding vacuum value (gray shaded band). The in-plasma peak reaches $\sim 2 \times 10^{23}\,\mathrm{W\,cm^{-2}}$ ($a_0 \approx 400$), while the vacuum peak is $\sim 8 \times 10^{21}\,\mathrm{W\,cm^{-2}}$ ($a_0 \approx 80$), demonstrating a 25-fold enhancement due to relativistic self-focusing and cavity confinement. Right axis: The instantaneous laser to particle species conversion efficiency vs time. The red, green, and violet lines correspond to electrons, ions, and photons, respectively; the integrated value is given on the label.

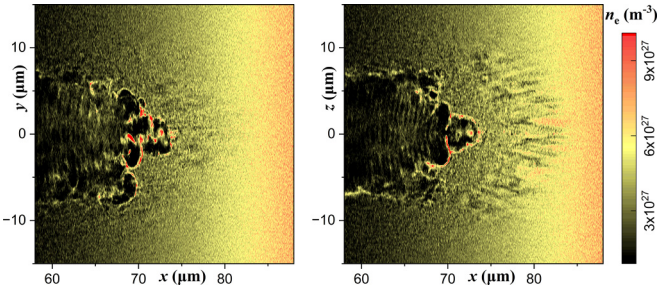

FIG. 3. Electron number density at a simulation time of 30 fs, showing the onset of small-scale filamentation driven by fast electrons. The xz plane on the right highlights that the filaments are more pronounced in the plane of the magnetic-field oscillation.

strong phase slippage, allowing sustained axial acceleration. Our QED-PIC simulations under these conditions yield electrons of $\sim$1.5 GeV, indicating a reasonably efficient coupling in the ultraintense regime.

Charge separation fields and return currents play non-negligible roles in shaping the beam-plasma dynamics [47]. As electrons are driven forward and expelled radially by the laser field, strong electrostatic sheath fields develop along the channel boundaries. These fields increase sharply and can reflect lower-energy electrons, triggering photon emission in the mid-energy range (tens of MeV). Enhancing that photon population is particularly significant for inducing photonuclear reactions, as their cross section peaks within that energy range.

At early times (lower density), our simulations reveal formation of distinct filamentary structures of smaller scale (comparable to the skin depth) ahead of the cavity boundary due to the fast electron population [48–50], characteristic of the Weibel-like current filamentation instability. These filaments emerge transversely to the laser propagation axis. The filamentation becomes more prominent at the plane of the magnetic-field oscillation, as seen in Fig. 3 at a simulation time of 30 fs. This behavior is consistent with recent experimental observations using long-wavelength lasers [51] and highlights the inherently collisionless nature of energy transport and instability growth in such regimes.

The onset of electron motion in near-critical plasmas coincides with the development of strong azimuthal magnetic fields generated by transverse current imbalances [52,53]. With an electron density of $\sim 5 \times 10^{26}\,\mathrm{m^{-3}}$ and a filament diameter of $\sim$1 μm (see Fig. 4), the enclosed current is $\sim 2 \times 10^4$ A, which by Ampère's law requires a pinching magnetic field of $\sim$7.5 kT at the filament edge. This simple estimate is in good agreement with the magnetic fields obtained in our simulations, which reach values of the order of tens of kilotesla in the filament vicinity. These self-generated fields exert a pinching force on the electron distribution, enhancing confinement within the cavity and eventually forming a low-density filament along the laser propagation axis, behind the main pulse [19,54,55]. In some simulations, we observe that in regions where hosing breaks the cavity symmetry, the magnetic topology becomes increasingly asymmetric, leading to randomized electron filamentation. Electron filamentation is

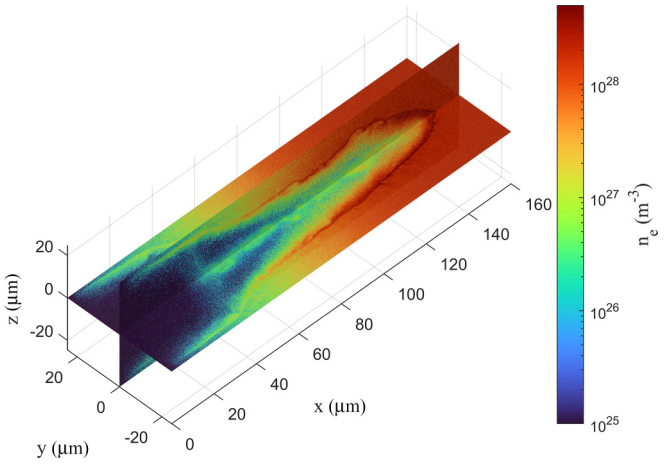

FIG. 4. Electron number density at the end of the simulation. Prominent feature is the long-lived central filament.

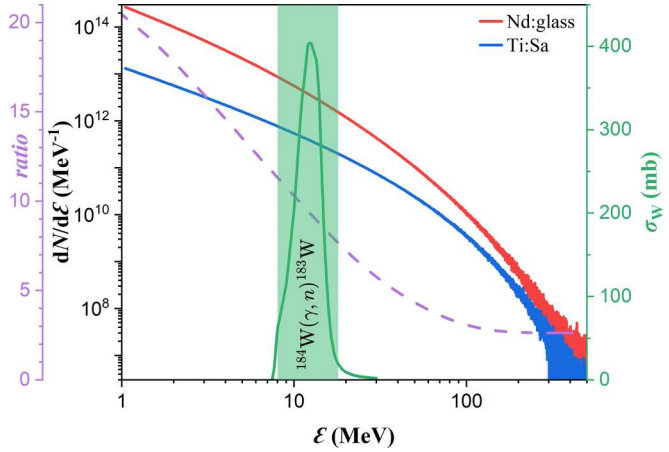

FIG. 5. Energy spectra of emitted photons from a 3D PIC simulation of an ultraintense laser interacting with a near-critical plasma. The red line corresponds to the present simulation using an Nd:glass laser system. The blue line compares results from a previous study using a Ti:Sa laser system [23]. Both lasers compared have a power of 10 PW. A broad distribution extending into the multi-MeV range is observed for both cases, but with the Nd:glass case yielding an order of magnitude more photons, as noted by the dashed purple line in the figure. The green line, highlighted by the green shaded region, indicates σ_{W} for the $^{184}\mathrm{W}(\gamma, n)^{183}\mathrm{W}$ reaction.

linked to ion filamentation in the center of the cavity, observed in proton probing experiments [56].

At around $0.5\,n_c$, a near-symmetric well-defined cavity forms on the xy plane, as shown in Fig. 1. On the xz plane, symmetry occurs along the laser propagation axis, but accompanied with formation of secondary distinct cavities, oriented roughly at 20°. In agreement with our simulation data, experimental observations show that often the cavity initially distorts due to partial filamentation, but quickly self-corrects [56], as evident by the extended cavity formed at the end of the simulation, seen in Fig. 4. The stable cavity formation results in the strong field amplification observed in our simulations and, consequently, peak γ-ray emission.

Angularly resolved photon spectra reveal two predominant emission lobes, centered at ±20° with respect to the laser propagation axis and each lobe corresponding to an approximate cone of 10° half-angle divergence. The evolution of laser intensity and photon conversion efficiency over time are shown by the black and red lines in Fig. 2, respectively. The photon energy spectrum extends up to 500 MeV, as shown in Fig. 5. The photon spectrum above 1 MeV is well fitted by

$$A_0 \exp\left(-\frac{\mathcal{E}}{\mathcal{E}_1}\right)\left[1+\left(\frac{\mathcal{E}}{\mathcal{E}_2}\right)^b\right]^{-k}, \tag{7}$$

with $A_0 = 1.6\times10^{17}\,\mathrm{MeV}^{-1}$, $\mathcal{E}_1 = 110\,\mathrm{MeV}$, $\mathcal{E}_2 = 100\,\mathrm{MeV}$, $k = 22.5$, and $b = 0.243$. The photon spectra of a previous study [dashed purple line in Fig. 4(b) of Ref. [23]] using a Ti:Sa laser of 10 PW power and 17 fs pulse duration are compared by the blue line in Fig. 5. In both studies, the electron density is chosen to be a fraction of n_{cr} to optimize γ yield. While tighter focusing in the Ti:Sa case leads to higher initial intensities, the longer pulse duration and higher energy of the Nd:glass laser support extended interaction and stronger self-focusing over the pulse length. This leads to an order of magnitude more photons being produced in the Nd:glass case, with comparable spectral cutoff energy, as shown by the ratio of the two spectra (dashed purple line). These results underline the suitability of kilojoule-class, longer-duration pulses for driving cavity-enhanced photon generation at high efficiency.

A laser in an undercritical plasma can excite a plasma wave that travels along the laser pulse, resulting in field self-modulation [57,58]. Moreover, when a laser is self-guided in a channel it can undergo a hosing instability. This instability results from a displacement of the centroid, causing the ponderomotive force to kink the plasma cavity. Since the laser is guided into lower-density regions, the misaligned plasma cavity enhances the laser centroid displacement, resulting in hosing instability. Thus, the propagation path of the laser is distorted and the cavity is modulated [59], thereby affecting electron acceleration and, consequently, the spatial characteristics of photon emission.

We examined the parametric behavior of the density profile on hosing instability by varying the amplitude n_{e0} and scale length w_0 of the electron density profile. We find that the γ-ray yield reaches its highest values for $0.3\,n_{\mathrm{cr}} < n_{e0} < 0.6\,n_{\mathrm{cr}}$ and $30\,\mu\mathrm{m} < w_0 < 50\,\mu\mathrm{m}$ (averaging at 17.6%). Within this parameter range, although strong photon yield occurs, no strict trend emerges, likely due to the stochastic nature of the hosing instability. We observe that slower gradients (larger w) along with lower n_{e0} values tend to enhance the growth of hosing and filamentation instabilities, as the laser pulse propagates further before dissipating its energy. On the other hand, steep gradients along with overly high n_{e0} suppress effective electron acceleration, thereby limiting photon emission. These results indicate that precise control over the preplasma profile provides a valuable lever for optimizing both photon yield and beam quality, with direct implications for experimental design on upcoming multipetawatt laser platforms.

Observation of side-scattered photons can provide a diagnostic of the plasma structure. In the case with no hosing

instability, $\pm 20^\circ$ cones are observed. The growth of transverse instabilities such as hosing and filamentation leaves clear imprints on the angular and spectral photon emission patterns. These emissions are modulated by the evolving cavity that directs the laser field, suggesting a pathway for using radiation signatures as probes of nonlinear laser-plasma dynamics. The spatiotemporal evolution of photon hotspots correlates strongly with the onset of channel deformation, indicating that diagnostic imaging of γ-ray profiles may serve as a sensitive tool for studying instability growth in near-critical-density plasmas.

To quantify the brightness and applicability of the emitted radiation, we compute the peak brilliance of the source at an emission angle of 20°. The source duration is 230 fs at FWHM, and the source size is approximately 1.4 μm (assumed as the region of the intensity FWHM at peak emission time). Thus, at 10 MeV photon energy the brightness is approximately 8×10^{22} photons/(s mm^2 mrad^2 0.1% BW), higher than proposed γ-ray emission schemes based on Ti:Sa lasers [23]. Our simulations indicate that a single laser shot can yield more than 4×10^{13} photons above 10 MeV, positioning this mechanism advantageously for inducing photonuclear reactions, whose cross sections peak around that energy. Importantly, the radiation is emitted from a micron-scale volume, allowing tight spatial localization and enabling compact experimental geometries for photonuclear studies [60–62].

To assess the feasibility for nuclear applications, we estimate the yield of photonuclear reactions induced by the emitted γ-ray pulses. We adopt known cross sections (averaged to $\langle\sigma_W\rangle = 200$ mbarn for photons of 8–18 MeV, highlighted by the green area in Fig. 5) for the $^{184}\mathrm{W}(\gamma, n)\,^{183}\mathrm{W}$ reaction [63] and assume a tungsten slab of thickness $l = 1$ cm. We calculate the tungsten number density, $n_W = N_A\,\rho_W/A \approx 6.3 \times 10^{22}\,\mathrm{cm}^{-3}$, where N_A is Avogadro's number, $\rho_W \approx 19.25\,\mathrm{g\,cm}^{-3}$ is tungsten mass density, and $A \approx 183.8\,\mathrm{g\,mol}^{-1}$ is tungsten atomic mass. By implementing $N_n = N_\gamma\, n_W\, \langle\sigma_W\rangle\, l$, we find that a single shot containing $N_\gamma = 3.8 \times 10^{13}$ photons of 8–18 MeV can generate more than 4.8×10^{11} photoneutrons in a compact secondary target. This opens opportunities for laser-driven nuclear diagnostics, isotope production, or ultrafast neutron radiography [64]. Additionally, the ultrashort duration and high energy of the source are attractive for time-resolved nuclear spectroscopy and probing QED pair creation thresholds in future setups with added background fields [2,65].

IV. CONCLUSIONS

In summary, we have demonstrated that kilojoule-class, moderately focused Nd:glass laser pulses interacting with near-critical plasmas can generate self-organized electron cavities that significantly enhance γ-ray production. The 3D simulations reveal that relativistic self-focusing and cavity formation increase the local laser amplitude by more than an order of magnitude, pushing the system into the strong radiation reaction regime and producing GeV-scale electrons and photons exceeding 500 MeV. The resulting γ-ray emission is directional, peaking around $\pm 20^\circ$, with laser-to-photon energy conversion efficiencies reaching up to 20%. These results underscore the importance of self-consistent channel dynamics and instabilities in shaping radiation output in realistic laser-plasma configurations. Unlike approaches relying on preformed channels, the self-organized nature of the cavity enables robust field amplification and high photon yield even under moderate focusing conditions. The interplay between relativistic transparency, radiation reaction, and dynamic cavity formation provides a scalable and experimentally accessible pathway to ultrabright, high-efficiency γ-ray sources in the multipetawatt regime.

ACKNOWLEDGMENTS

This work was supported by the project "Advanced research using high intensity laser produced photons and particles" (ADONIS) (CZ.02.1.01/0.0/0.0/16_019/0000789) from the European Regional Development Fund. C.P.R. acknowledges support from EPSRC grant EP/V049461/1. The epoch code is in part funded by the UK EPSRC Grants No. EP/G054950/1, No. EP/G056803/1, No. EP/G055165/1, and No. EP/M022463/1.

DATA AVAILABILITY

The data that support the findings of this article are not publicly available upon publication because it is not technically feasible and/or the cost of preparing, depositing, and hosting the data would be prohibitive within the terms of this research project. The data are available from the authors upon reasonable request.

[1] D. Strickland and G. Mourou, Compression of amplified chirped optical pulses, Opt. Commun. **56**, 219 (1985).

[2] A. Di Piazza, C. Müller, K. Z. Hatsagortsyan, and C. H. Keitel, Extremely high-intensity laser interactions with fundamental quantum systems, Rev. Mod. Phys. **84**, 1177 (2012).

[3] A. Gonoskov, T. G. Blackburn, M. Marklund, and S. S. Bulanov, Charged particle motion and radiation in strong electromagnetic fields, Rev. Mod. Phys. **94**, 045001 (2022).

[4] T. Nakamura, J. K. Koga, T. Z. Esirkepov, M. Kando, G. Korn, and S. V. Bulanov, High-power γ-ray flash generation in ultraintense laser-plasma interactions, Phys. Rev. Lett. **108**, 195001 (2012).

[5] C. P. Ridgers, C. S. Brady, R. Duclous, J. G. Kirk, K. Bennett, T. D. Arber, A. P. L. Robinson, and A. R. Bell, Dense electron-positron plasmas and ultraintense γ rays from laser-irradiated solids, Phys. Rev. Lett. **108**, 165006 (2012).

[6] F. Niel, C. Riconda, F. Amiranoff, R. Duclous, and M. Grech, From quantum to classical modeling of radiation reaction: A focus on stochasticity effects, Phys. Rev. E **97**, 043209 (2018).

[7] T. G. Blackburn, Radiation reaction in electron–beam interactions with high-intensity lasers, Rev. Mod. Plasma Phys. **4**, 5 (2020).

[8] P. Hadjisolomou, T. M. Jeong, D. Kolenaty, A. J. Macleod, V. Olšovcová, R. Versaci, C. P. Ridgers, and S. V. Bulanov,

Gamma-flash generation in multi-petawatt laser–matter interactions, Phys. Plasmas **30**, 093103 (2023).

[9] K. W. D. Ledingham, I. Spencer, T. McCanny, R. P. Singhal, M. I. K. Santala, E. Clark, I. Watts, F. N. Beg, M. Zepf, K. Krushelnick *et al.*, Photonuclear physics when a multiterawatt laser pulse interacts with solid targets, Phys. Rev. Lett. **84**, 899 (2000).

[10] V. G. Nedorezov, A. A. Turinge, and Y. M. Shatunov, Photonuclear experiments with Compton-backscattered gamma beams, Phys. Usp. **47**, 341 (2004).

[11] C. Müller, A. Di Piazza, A. Shahbaz, T. J. Bürvenich, J. Evers, K. Z. Hatsagortsyan, and C. H. Keitel, High-energy, nuclear, and QED processes in strong laser fields, Laser Phys. **18**, 175 (2008).

[12] M. J. Rees and P. Mészáros, Relativistic fireballs: Energy conversion and time-scales, Mon. Not. R. Astron. Soc. **258**, 41P (1992).

[13] R. Ruffini, G. Vereshchagin, and S. S. Xue, Electron–positron pairs in physics and astrophysics: From heavy nuclei to black holes, Phys. Rep. **487**, 1 (2010).

[14] S. V. Bulanov, T. Z. Esirkepov, M. Kando, J. Koga, K. Kondo, and G. Korn, On the problems of relativistic laboratory astrophysics and fundamental physics with super powerful lasers, Plasma Phys. Rep. **41**, 1 (2015).

[15] A. A. Philippov and A. Spitkovsky, *Ab initio* pulsar magnetosphere: Particle acceleration in oblique rotators and high-energy emission modeling, Astrophys. J. **855**, 94 (2018).

[16] F. Aharonian, Q. An, Axikegu, L. X. Bai, Y. X. Bai, Y. W. Bao, D. Bastieri, X. J. Bi, Y. J. Bi, H. Cai *et al.* (LHAASO Collaboration), Extended very-high-energy gamma-ray emission surrounding PSR J0622 + 3749 observed by LHAASO−KM2A, Phys. Rev. Lett. **126**, 241103 (2021).

[17] A. J. MacLeod, P. Hadjisolomou, T. M. Jeong, and S. V. Bulanov, All-optical nonlinear Breit-Wheeler pair production with γ-flash photons, Phys. Rev. A **107**, 012215 (2023).

[18] M. Mirzaie, C. I. Hojbota, D. Y. Kim, V. B. Pathak, T. G. Pak, C. M. Kim, H. W. Lee, J. W. Yoon, S. K. Lee, Y. J. Rhee, M. Vranic, Ó. Amaro, K. Y. Kim, J. H. Sung, and C. H. Nam, All-optical nonlinear Compton scattering performed with a multi-petawatt laser, Nat. Photon. **18**, 1212 (2024).

[19] A. Pukhov, Z. M. Sheng, and J. Meyer-ter Vehn, Particle acceleration in relativistic laser channels, Phys. Plasmas **6**, 2847 (1999).

[20] A. V. Arefiev, A. P. L. Robinson, and V. N. Khudik, Novel aspects of direct laser acceleration of relativistic electrons, J. Plasma Phys. **81**, 475810404 (2015).

[21] P. Hadjisolomou, T. M. Jeong, P. Valenta, G. Korn, and S. V. Bulanov, Gamma-ray flash generation in irradiating a thin foil target by a single-cycle tightly focused extreme power laser pulse, Phys. Rev. E **104**, 015203 (2021).

[22] K. Sugimoto, Y. He, N. Iwata, I. L. Yeh, K. Tangtartharakul, A. Arefiev, and Y. Sentoku, Positron generation and acceleration in a self-organized photon collider enabled by an ultraintense laser pulse, Phys. Rev. Lett. **131**, 065102 (2023).

[23] P. Hadjisolomou, T. M. Jeong, and S. V. Bulanov, Towards bright gamma-ray flash generation from tailored target irradiated by multi-petawatt laser, Sci. Rep. **12**, 17143 (2022).

[24] C. Yu, R. Qi, W. Wang, J. Liu, W. Li, C. Wang, Z. Zhang, J. Liu, Z. Qin, M. Fang *et al.*, Ultrahigh brilliance quasi-monochromatic MeV γ-rays based on self-synchronized all-optical compton scattering, Sci. Rep. **6**, 29518 (2016).

[25] T. W. Huang, C. M. Kim, C. T. Zhou, M. H. Cho, K. Nakajima, C. M. Ryu, S. C. Ruan, and C. H. Nam, Highly efficient laser-driven Compton gamma-ray source, New J. Phys. **21**, 013008 (2019).

[26] M. Galbiati, A. Formenti, M. Grech, and M. Passoni, Numerical investigation of non-linear inverse Compton scattering in double-layer targets, Front. Phys. **11**, 1117543 (2023).

[27] T. Esirkepov, M. Borghesi, S. V. Bulanov, G. Mourou, and T. Tajima, Highly efficient relativistic-ion generation in the laser-piston regime, Phys. Rev. Lett. **92**, 175003 (2004).

[28] K. V. Lezhnin, P. V. Sasorov, G. Korn, and S. V. Bulanov, High power gamma flare generation in multi-petawatt laser interaction with tailored targets, Phys. Plasmas **25**, 123105 (2018).

[29] P. Hadjisolomou, I. P. Tsygvintsev, P. Sasorov, V. Gasilov, G. Korn, and S. V. Bulanov, Preplasma effects on laser ion generation from thin foil targets, Phys. Plasmas **27**, 013107 (2020).

[30] C. N. Danson, C. Haefner, J. Bromage, T. Butcher, J. F. Chanteloup, E. A. Chowdhury, A. Galvanauskas, L. A. Gizzi, J. Hein, D. I. Hillier *et al.*, Petawatt and exawatt class lasers worldwide, High Power Laser Sci. **7**, e54 (2019).

[31] B. Rus, P. Bakule, R. Antipenkov, T. Green, P. Szotkowski, J. Novák, P. Trojek, S. Vyhlídka, L. Haizer, and D. Kramer, ELI beamlines lasers: Status update, in *High-Power, High-Energy Lasers, and Ultrafast Optical Technologies II*, edited by P. Bakule, P. Baer, J. Hein, and T. J. Butcher (SPIE, Bellingham, Washington, USA, 2025), Vol. PC13532, p. PC135320E.

[32] G. A. Askaryan, Effect of the gradient of a strong electromagnetic ray on electrons and atoms, Sov. Phys. JETP **15**, 1088 (1962).

[33] R. Y. Chiao, E. Garmire, and C. H. Townes, Self-trapping of optical beams, Phys. Rev. Lett. **13**, 479 (1964).

[34] P. L. Kelley, Self-focusing of optical beams, Phys. Rev. Lett. **15**, 1005 (1965).

[35] G. Z. Sun, E. Ott, Y. C. Lee, and P. Guzdar, Self-focusing of short intense pulses in plasmas, Phys. Fluids **30**, 526 (1987).

[36] S. V. Bulanov, V. A. Vshivkov, G. I. Dudnikova, E. T. Z., F. Califano, F. F. Kamenets, T. V. Liseikina, N. M. Naumova, and F. Pegoraro, Interaction of petawatt laser pulses with underdense plasmas, Plasma Phys. Rep. **25**, 701 (1999).

[37] V. Sazegari, M. Mirzaie, and B. Shokri, Ponderomotive acceleration of electrons in the interaction of arbitrarily polarized laser pulse with a tenuous plasma, Phys. Plasmas **13**, 033102 (2006).

[38] P. Zhang, C. P. Ridgers, and A. G. R. Thomas, The effect of nonlinear quantum electrodynamics on relativistic transparency and laser absorption in ultra-relativistic plasmas, New J. Phys. **17**, 043051 (2015).

[39] T. D. Arber, K. Bennett, C. S. Brady, A. Lawrence-Douglas, M. G. Ramsay, N. J. Sircombe, P. Gillies, R. G. Evans, H. Schmitz, A. R. Bell *et al.*, Contemporary particle-in-cell approach to laser-plasma modelling, Plasma Phys. Control. Fusion **57**, 113001 (2015).

[40] M. Sachithanadam and S. C. Joshi, High strain recovery with improved mechanical properties of gelatin–silica aerogel composites post-binding treatment, J. Mater. Sci. **49**, 163 (2014).

[41] J. C. H. Wong, H. Kaymak, S. Brunner, and M. M. Koebel, Mechanical properties of monolithic silica aerogels made from polyethoxydisiloxanes, Microporous Mesoporous Mater. **183**, 23 (2014).

[42] S. Iswar, S. Galmarini, L. Bonanomi, J. Wernery, E. Roumeli, S. Nimalshantha, A. M. Ben Ishai, M. Lattuada, M. M. Koebel, and W. J. Malfait, Dense and strong, but superinsulating silica aerogel, Acta Mater. **213**, 116959 (2021).

[43] A. V. Higuera and J. R. Cary, Structure-preserving second-order integration of relativistic charged particle trajectories in electromagnetic fields, Phys. Plasmas **24**, 052104 (2017).

[44] C. Gahn, G. D. Tsakiris, A. Pukhov, J. Meyer-ter Vehn, G. Pretzler, P. Thirolf, D. Habs, and K. J. Witte, Multi-MeV electron beam generation by direct laser acceleration in high-density plasma channels, Phys. Rev. Lett. **83**, 4772 (1999).

[45] A. G. York, H. M. Milchberg, J. P. Palastro, and T. M. Antonsen, Direct acceleration of electrons in a corrugated plasma waveguide, Phys. Rev. Lett. **100**, 195001 (2008).

[46] E. Esarey, P. Sprangle, and J. Krall, Laser acceleration of electrons in vacuum, Phys. Rev. E **52**, 5443 (1995).

[47] M. Passoni, V. T. Tikhonchuk, M. Lontano, and V. Y. Bychenkov, Charge separation effects in solid targets and ion acceleration with a two-temperature electron distribution, Phys. Rev. E **69**, 026411 (2004).

[48] C. Ren, M. Tzoufras, F. S. Tsung, W. B. Mori, S. Amorini, R. A. Fonseca, L. O. Silva, J. C. Adam, and A. Heron, Global simulation for laser-driven MeV electrons in fast ignition, Phys. Rev. Lett. **93**, 185004 (2004).

[49] M. Tzoufras, C. Ren, F. S. Tsung, J. W. Tonge, W. B. Mori, M. Fiore, R. A. Fonseca, and L. O. Silva, Space-charge effects in the current-filamentation or Weibel instability, Phys. Rev. Lett. **96**, 105002 (2006).

[50] S. V. Bulanov, T. Z. Esirkepov, M. Kando, F. Pegoraro, S. S. Bulanov, C. G. R. Geddes, C. B. Schroeder, E. Esarey, and W. P. Leemans, Ion acceleration from thin foil and extended plasma targets by slow electromagnetic wave and related ion-ion beam instability, Phys. Plasmas **19**, 103105 (2012).

[51] N. P. Dover, O. Tresca, N. Cook, O. C. Ettlinger, R. J. Kingham, C. Maharjan, M. N. Polyanskiy, P. Shkolnikov, I. Pogorelsky, and Z. Najmudin, Optical imaging of laser-driven fast electron Weibel-like filamentation in overcritical density plasma, Phys. Rev. Lett. **134**, 025102 (2025).

[52] T. Z. Esirkepov, Y. Sentoku, K. Mima, K. Nishihara, F. Califano, F. Pegoraro, N. M. Naumova, S. V. Bulanov, Y. Ueshima, T. V. Liseikina *et al.*, Ion acceleration by superintense laser pulses in plasmas, JETP Lett. **70**, 82 (1999).

[53] J. Park, S. S. Bulanov, J. Bin, Q. Ji, S. Steinke, J. L. Vay, C. G. R. Geddes, C. B. Schroeder, W. P. Leemans, T. Schenkel, and E. Esarey, Ion acceleration in laser generated megatesla magnetic vortex, Phys. Plasmas **26**, 103108 (2019).

[54] K. Jiang, A. Pukhov, and C. T. Zhou, Magnetic field amplification to gigagauss scale via hydrodynamic flows and dynamos driven by femtosecond lasers, New J. Phys. **23**, 063054 (2021).

[55] P. Valenta, D. Maslarova, R. Babjak, B. Martinez, S. V. Bulanov, and M. Vranić, Direct laser acceleration: A model for the electron injection from the walls of a cylindrical guiding structure, Phys. Rev. E **109**, 065204 (2024).

[56] L. Willingale, P. M. Nilson, A. G. R. Thomas, J. Cobble, R. S. Craxton, A. Maksimchuk, P. A. Norreys, T. C. Sangster, R. H. H. Scott, C. Stoeckl *et al.*, High-power, kilojoule class laser channeling in millimeter-scale underdense plasma, Phys. Rev. Lett. **106**, 105002 (2011).

[57] P. Sprangle, E. Esarey, J. Krall, and G. Joyce, Propagation and guiding of intense laser pulses in plasmas, Phys. Rev. Lett. **69**, 2200 (1992).

[58] P. Sprangle, J. Krall, and E. Esarey, Hose-modulation instability of laser pulses in plasmas, Phys. Rev. Lett. **73**, 3544 (1994).

[59] L. Ceurvorst, N. Ratan, M. C. Levy, M. F. Kasim, J. Sadler, R. H. H. Scott, R. M. G. M. Trines, T. W. Huang, M. Skramic, M. Vranic *et al.*, Mitigating the hosing instability in relativistic laser-plasma interactions, New J. Phys. **18**, 053023 (2016).

[60] H. Y. Lan, D. Wu, J. X. Liu, J. Y. Zhang, H. G. Lu, J. F. Lv, X. Z. Wu, W. Luo, and X. Q. Yan, Photonuclear production of nuclear isomers using bremsstrahlung induced by laser-wakefield electrons, Nucl. Sci. Tech. **34**, 74 (2023).

[61] D. Wu, H. Y. Lan, J. Y. Zhang, J. X. Liu, H. G. Lu, J. F. Lv, X. Z. Wu, H. Zhang, J. Cai, X. L. Xu *et al.*, New measurements of ^{92}Mo(γ, n) and (γ, 3n) reactions using laser-driven bremsstrahlung γ-ray, Front. Phys. **11**, 1178257 (2023).

[62] F. A. Rasulova, N. V. Aksenov, S. I. Alekseev, S. S. Belyshev, I. Chuprakov, N. Y. Fursova, A. S. Madumarov, J. H. Khushvaktov, and A. A. Kuznetsov, Photonuclear reactions on stable isotopes of molybdenum at bremsstrahlung endpoint energies of 10–23 MeV, Phys. Rev. C **111**, 024604 (2025).

[63] A. J. Koning, D. Rochman, J. C. Sublet, N. Dzysiuk, M. Fleming, and S. van der Marck, TENDL: Complete nuclear data library for innovative nuclear science and technology, Nucl. Data Sheets **155**, 1 (2019).

[64] M. Roth, D. Jung, K. Falk, N. Guler, O. Deppert, M. Devlin, A. Favalli, J. Fernandez, D. Gautier, M. Geissel *et al.*, Bright laser-driven neutron source based on the relativistic transparency of solids, Phys. Rev. Lett. **110**, 044802 (2013).

[65] A. Gonoskov, A. Bashinov, S. Bastrakov, E. Efimenko, A. Ilderton, A. Kim, M. Marklund, I. Meyerov, A. Muraviev, and A. Sergeev, Ultrabright GeV photon source via controlled electromagnetic cascades in laser-dipole waves, Phys. Rev. X **7**, 041003 (2017).